JACS
JOURNAL OF THE AMERICAN CHEMICAL SOCIETY

ARTICLE

pubs.acs.org/JACS

Multifunctional Surface Modification of Gold-Stabilized Nanoparticles by Bioorthogonal Reactions

Xiuru Li, Jun Guo, Jinkeng Asong, Margreet A. Wolfert, and Geert-Jan Boons*

Complex Carbohydrate Research Center, University of Georgia, 315 Riverbend Road, Athens, Georgia 30602, United States

Supporting Information

ABSTRACT: Nanocarriers that combine multiple properties in an all-in-one system hold great promise for drug delivery. The absence of technology to assemble highly functionalized devices has, however, hindered progress in nanomedicine. To address this deficiency, we have chemically synthesized poly(ethylene oxide)-β-poly(ε-caprolactone) (PEO-*b*-PCL) block polymers modified at the apolar PCL terminus with thioctic acid and at the polar PEO terminus with an acylhydrazide, amine, or azide moiety. The resulting block polymers were employed to prepare nanoparticles that have a gold core, an apolar polyester layer for drug loading, a polar PEO corona to provide biocompatibility, and three different types of surface reactive groups for surface functionalization. The acylhydrazide, amine, or azide moieties of the resulting nanoparticles could be reacted with high efficiencies with modules having a ketone, isocyanate, or active ester and alkyne function, respectively. To demonstrate proof of principle of the potential of multisurface functionalization, we prepared nanoparticles that have various combinations of an oligo-arginine peptide to facilitate cellular uptake, a histidine-rich peptide to escape from lysosomes, and an Alexa Fluor 488 tag for imaging purposes. It has been shown that uptake and subcellular localization of the nanoparticles can be controlled by multisurface modification. It is to be expected that the modular synthetic methodology provides unique opportunities to establish optimal configurations of nanocarriers for disease-specific drug delivery.

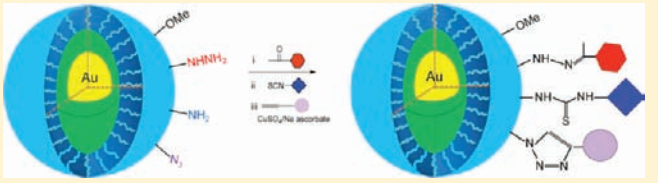

INTRODUCTION

Nanomaterials, such as liposomes, organomicelles, and gold nanoparticles, are emerging as promising devices for drug and gene delivery.[1−4] These carriers can increase longevity of a drug in the bloodstream, solubilize a hydrophobic drug, offer controlled release by environmental sensitive or external stimuli, and accumulate in solid tumors by enhanced permeability and retention effect.[5] The therapeutic efficiency of nanomaterials can be further improved by surface functionalization by, for example, a tissue targeting ligand,[6] a cell-penetrating molecule,[7] or a signaling peptide for organelle targeting.[8] Moreover, therapeutic targeting can be combined with imaging by attachment of an appropriate contrast agent.[4]

Multifunctional nanocarriers that combine several properties, such as tissue targeting, cell entry, organelle-specific delivery, and imaging, in an all-in-one system are expected to offer a multimodal approach for enhanced efficacy of many therapeutics and diagnostics.[9,10] A major hurdle in the development of such devices is, however, a lack of robust chemical technology for the preparation of nanoparticles that can be modified at their surfaces with various functional modules and possess other properties, such as biological stealthiness, drug loading capacity, selective release, and imaging capabilities. Herein, we describe a versatile chemical approach for selective surface modification of nanoparticles using three bioorthogonal coupling reactions. To implement the new approach, nanoparticles were prepared that have a gold core modified with a monolayer of poly(ethylene oxide)-β-poly(ε-caprolactone) (PEO-*b*-PCL) block polymers. The block polymers were modified at the PCL terminus with a thioctic acid moiety for covalent attachment to the gold core and at the PEO terminus with acylhydrazides, amines, and azides for coupling with functional modules having a ketone, isocyanate, or active ester and alkyne, respectively. The gold core of the nanoparticles was expected to provide stability during synthesis, ensure controlled degradation after cellular uptake, and offer an opportunity for imaging. Furthermore, the apolar polyester layer of the nanoparticles offers a loading space for apolar drugs, and the poly(ethylene oxide) (PEO) corona provides biocompatibility and biological stealthiness.[11] The synthetic strategy is highly modular, and from a single nanoparticle platform, many different combinations of surface modules can be attached, opening important new avenues to establish optimal configuration for targeted delivery of pharmaceuticals. As a proof of principle, we have prepared and biologically evaluated nanoparticles loaded with a cytotoxic drug and modified with various combinations of a cell permeation peptide for improving cellular uptake, a histidine-rich peptide for lysosomal escape, and a fluorescent label for quantification and have demonstrated that by multisurface modification, uptake, and subcellular localization can be controlled.

RESULTS AND DISCUSSION

Chemical Synthesis of Functionalized Block Polymers. Amphiphilic block polymers composed of PEO-*b*-PCL assemble

Received: February 8, 2011
Published: June 16, 2011

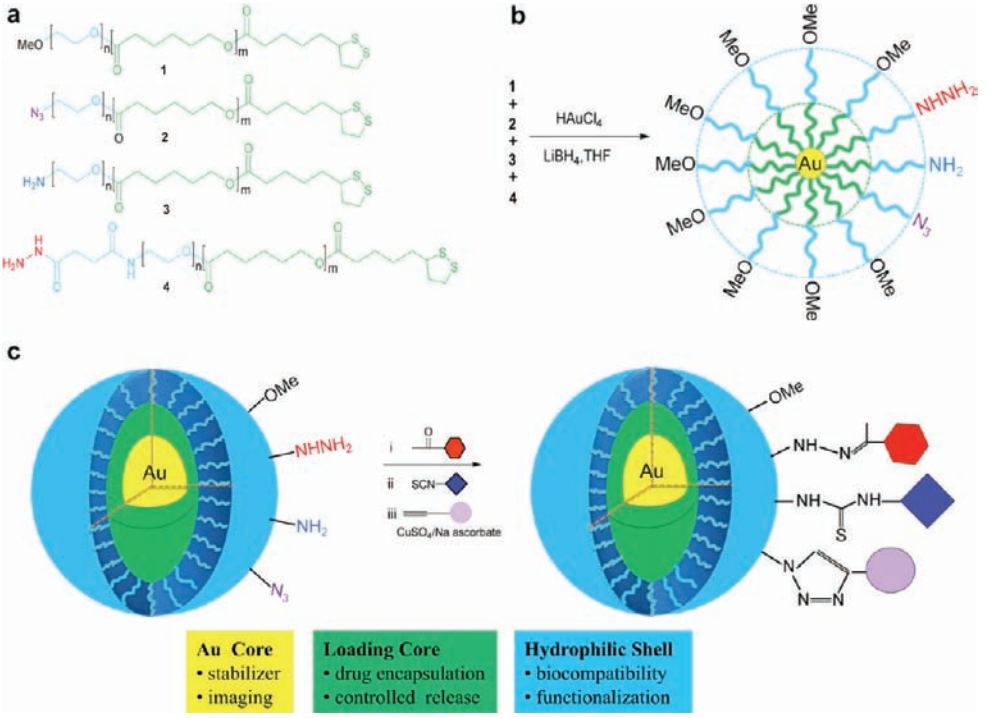

Figure 1. Chemical synthesis of multifunctional gold-stabilized nanoparticles. The structure of block polymers modified at the apolar PCL end with thioic acid moiety for attachment to a gold core and at the PEO terminus with a functional group for post synthesis modification (a). The chemical synthesis of multifunctional nanoparticles by a modified Brust method (b). A cartoon of the architecture of the nanopaticles in aqueous solution and the three sequential bioorthogonal reactions for surface modification (c). The nanoparticles have an inner gold core (yellow) that provides stabilization, controlled degradation, and opportunity for imaging with TEM. The apolar PCL layer (green) provides a loading space for apolar compounds, and the hydrophilic PEO shell (blue) offers biocompatibility. Three different surface functional groups are present for post-synthesis modification. First, the acylhydrazides react selectively with ketones to give a hydrazone-linked modules. Next, the amines react with isocyanates or active ester at pH of 8−9 to give thioureas or amides, respectively, and finally, azides are reacted with alkynes in the presence of Cu(I) to provide triazole-linked modules.

in water into polymeric micelles that can carry lipophilic drugs, such as FK506 and dihydrotestosterone.[3] It was envisaged that polymeric micelles carrying acylhydrazide, amine, and azide at the polar PEO terminus (compounds **2**−**4**, Figure 1) will make it possible to modify the surface in a sequential manner with modules containing a ketone, isocyanate, or active ester and alkyne, respectively. These coupling reactions have been employed in bioconjugation[12] and were expected to be selective when performed in an appropriate order. The additional use of a PEO-*b*-PCL derivative, containing a terminal nonreactive methyl ether (compound **1**), will make it possible to control the density of the various reactive functionalities at the nanoparticle surface. Previously, it was found that an appropriate density of a surface module may be important for optimal targeting efficiency.[13] Furthermore, modification of the apolar PCL terminus of the block polymers with thioctic acid should offer an opportunity to attach the polymers in a controlled fashion to a gold nanoparticle core.[14,15] It was expected that the resulting gold-stabilized nanoparticles would be sufficiently stable to undergo several chemical modifications without affecting the structural integrity of the particles. In this respect, preliminary studies had shown that micelles formed from N_3-PEO-*b*-PCL block polymers disassemble upon attachment of charged modules, such as arginine-rich peptides. Furthermore, we found that even when neutral modules were employed, N_3-PEO-*b*-PCL micelles were not sufficiently stable to undergo several chemical modification and purification steps. In addition to providing stability, the gold core is expected to facilitate controlled degradation of the particles after cell entry by displacement of the gold-linked polymers by glutathione,[16] which is present at high concentration in the intracellular environment and provides opportunities for imaging.

Functionalized polymers **1** and **2** were prepared by a strategy in which caprolactone was polymerized using methoxy- (**5**) and azido-polyethylene glycol (**8**) (*Mn* ∼ 2000 Da) as the macroinitiator to give block polymers **6** and **9**, respectively, which have a hydroxyl at the PCL terminus that provided an opportunity to install selectively a thioctic acid moiety. Azido-polyethylene glycol (**8**) was prepared by treatment of commercially available ethylene glycol with tosyl chloride (1 equiv) in a mixture of dichloromethane and pyridine, followed by reaction of the crude product with sodium azide in DMF at 80 °C. As expected, a small amount of a diazido derivative and starting material was formed, which could easily be removed by traditional silica gel column chromatography to give **8** in an overall yield of 58%. The structure of **8** was confirmed by a combination of matrix-assisted laser desorption/ionization time-of-flight mass spectrometry (MALDI-TOF MS), Fourier-transform infrared (FT-IR), and ^{1}H NMR measurements. Thus, a stretching vibration at ∼2098 cm^{-1} in the FT-IR spectrum of **8** indicated the presence of the azido group. Furthermore, the ^{1}H NMR spectrum showed that the protons of the methylene moiety adjacent to the hydroxyl had an appropriate relative integration, and the MALDI-TOF MS spectrum of **8** showed that all molecular ions had an increase of 25 mass units compared to corresponding signals in the MS spectrum of **7**, indicating full conversion of a hydroxyl into an azido moiety (Figures S1 and S2, Supporting Information).

Scheme 1. Chemical Synthesis of Compounds 1−4[a]

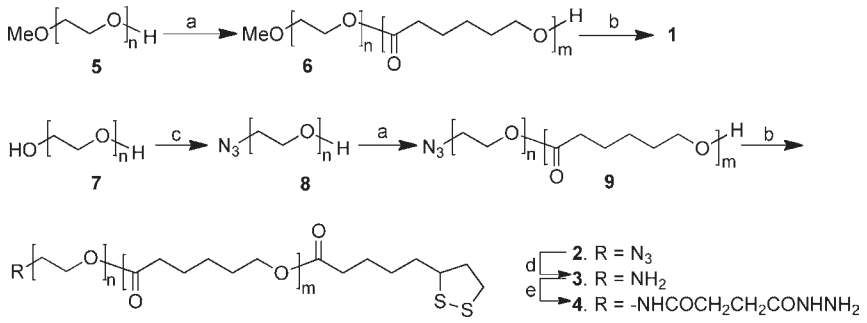

[a] (a)Reagents and conditions: ε-caprolactone, SnOct, 130 °C; (b) thioctic acid, DCC, DMAP, Et_3N, CH_2Cl_2; (c): TsCl, pyridine, CH_2Cl_2, ii) NaN_3, DMF, 80 °C; (d) Ph_3P, THF, H_2O; (e) 4-(*N′-tert*-butoxycarbonyl-hydrazino)-4-oxo-butyric acid, DCC, DMAP, CH_2Cl_2, ii) 20% TFA, CH_2Cl_2.

Table 1. Molecular Weight of Polymers 1−4

	^{1}H NMR	SEC	
polymers	$\overline{M}$n[a] (Da)	$\overline{M}$n[b] (Da)	PDI[b]
1	4700	6070	1.42
2	5220	7400	1.38
3	5200	7420	1.35
4	5288	7500	1.30

[a] The number-average molecular weight ($\overline{M}$n) was determined by ^{1}H NMR. [b] $\overline{M}$n and polydispersity index (PDI) were measured by SEC; PDI is the ratio of weight-average molecular weight $\overline{M}$w and $\overline{M}$n. The difference in the molecular weight obtained by SEC and ^{1}H NMR is related to differences in the hydrodynamic volume of the polymer in chloroform compared to polystyrene standards. ^{1}H NMR provides a more accurate method for average molecular weight determination.

Next, a ring-opening polymerization was performed by heating a mixture of caprolactone, a catalytic amount of tin(II) 2-ethylhexanoate (SnOct) and polyethylene glycol derivatives **5** and **8** as the macroinitiator in a sealed tube at 130 °C for 24 h[17] to give, after purification by precipitation in hexane, block polymers **6** and **9**, respectively. The polymerization had resulted in the formation of a hydroxyl at the polyester terminus, which was used to selectively introduce a thioctic acid moiety. Thus, treatment of **6** and **9** with thioctic acid in the presence of *N,N′*-dicyclohexylcarbodiimide (DDC), 4-(dimethylamino) pyridine (DMAP), and triethyl amine (Scheme 1) lead to the formation of functionalized block polymers **1** and **2**, respectively. FT-IR confirmed the presence of the azido moiety (2098 cm^{-1}) of compound **2** (Figure S6, Supporting Information), and the ^{1}H NMR spectrum of **1** and **2** showed that the proton signals of the methylene group adjacent to the S−S bond of the thioctate moiety (3.05−3.20 ppm) had appropriate relative integrations (compared to the terminal methoxy group) indicating fully functionalized with a thioctic acid moiety.

Compound **2** was the starting material for the preparation of amine **3** by reduction of the azido moiety with triphenyl phosphine in a mixture of THF and water. Acylhydrazide-modified **4** was obtained by acylation of the amine of **3** with 4-(*N′-tert*-butoxycarbonyl-hydrazino)-4-oxo-butyric acid followed by removal of the Boc protecting group using 20% TFA in DCM.

Analysis of the polymers **1**−**4** by ^{1}H NMR and size exclusion chromatography (SEC) gave a number average molecular weight (*M*n) of 4700−5288 Da and a PDI of 1.30−1.42 (Table 1). The

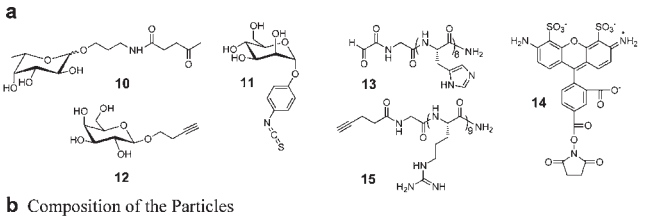

b Composition of the Particles

Particles	Starting compositions (%)				Surface modifications (%)					
	1	**2**	**3**	**4**	**10**	**11**	**12**	**13**	**14**	**15**
A	70	10	10	10						
B	100									
C	70	10	10	10	9.1	8.1	7.8			
D	70	10	10	10					6.2	
E	70	10	10	10					6.2	5.5
F	70	10	10	10				8.0	6.2	5.5
G	70	10	10	10				8.0		5.5

Figure 2. Modules for surface modification and chemical composition of nanoparticles. The chemical structures of compounds **10**−**15** used for surface modification of the nanoparticles (a). The chemical compositions of the various nanoparticles (b).

data demonstrate that the transformation of **2** into **3** and **4** does not alter the molecular weight distribution, indicating that the employed reaction conditions are compatible with the ester groups of the PCL backbone.

Nanoparticle Preparation. Gold nanoparticles **A** covered with amphiphilic block polymers (Figures 1 and 2), and having three different surface reactive functional groups, were prepared by the addition of $LiBH_4$ to a vigorously stirred mixture of block polymers **1**−**4** and $HAuCl_4$ in anhydrous THF. The reducing agent induced an immediate color change from yellow to deep purple indicating that gold nanoparticles had been formed. After a reaction time of 3 h, methanol was added to quench the excess of $LiBH_4$.[14,15] It was found that the resulting surface-modified gold nanoparticles were soluble in THF, which made it possible to remove uncomplexed polymers and inorganic salts by dialyzing against THF. As a control experiment, free polymer was dialyzed against THF, and the absence of polymeric material in the resulting solution confirmed that the dialysis procedure efficiently removes uncomplexed material.

An aqueous solution of nanoparticles was obtained by partial concentration of the organic solution, followed by the addition of

water and the extensive dialysis against water. Dynamic light scattering showed that the resulting nanoparticles have a narrow size distribution and an average diameter of 33 ± 8 nm (Figure S14, Supporting Information). Furthermore, transmission electron microscopy (TEM) images revealed that the gold core had an average diameter of ~5 nm, and a signal at 2098 cm^{-1} in the IR spectrum (stretching vibration of azide) confirmed the presence of azido groups (Figures S9, S11, and S12, Supporting Information). A similar procedure was employed to prepare nanoparticles **B** by only employing block polymer **1**. Thermogravimetric analyses (TGA) of **A** and **B** gave a weight ratio of gold to organic matter of 6:94, which indicates that a significant percentage of polymers is not chemically anchored to the gold core (Figure S16, Supporting Information). Interestingly, aggregates of gold nanoparticles were formed when a PCL-PEO block polymer lacking a disulfide moiety was employed in the procedure for gold-stabilized nanoparticle preparation. Thus, the thioctic acid moiety of the block polymers is critical for the formation of stable nanoparticles. It is possible that polymeric molecules that are not chemically anchored to the surface of the gold core are held in place by polymers that are covalently linked to the gold core. In this respect, PCL is semicrystalline at ambient temperature,[15] and thus it is likely that covalently linked and unlinked material form a strong lattice resulting in stable nanoparticles. However, the issue of higher than expected ratio of polymer to gold is not fully resolved, as dialysis against THF should have removed all unbound polymer, yet TEM images (Figures S13, S15 and S17, Supporting Information) show structural heterogeneity with some nanoparticles appearing to lack a gold core.

To establish conditions for the selective conjugation, fucoside **10**, mannoside **11**, and galactoside **12**, having a ketone, isocyanate, and alkyne moiety, respectively, were sequentially conjugated to the gold-stabilized nanoparticles **A**. Thus, ketone **10** was added to an aqueous solution of nanoparticles **A** for reaction with the surface acylhydrazides to form acylhydrazone linkages. After a reaction time of 24 h, the pH was adjusted to ~8 by adding aqueous $NaHCO_3$, and the isocyanate **11** was added for reaction with the surface amines to form stable thioureas. After stirring for an additional 24 h, the solution was dialyzed against water, and then a Cu(I)-catalyzed reaction was performed between the alkyne of **12** and the azides of the nanoparticles to form triazoles,[18] and after, dialysis trifunctionalized **C** was obtained (Figure 2). Analysis by light scattering and TEM indicated no significant change in size, and morphology had occurred during the chemical transformations (Figure S15, Supporting Information). Furthermore, quantitative sugars analysis by treatment of the particles with TFA to hydrolyze glycosidic linkages followed by monosaccharide analysis by high pH anion exchange chromatography (HPAEC) showed that the fucoside, mannoside, and galactoside had been incorporated with efficiencies of 91, 81, and 78%, respectively (Figure S18, Supporting Information). When the same procedure was applied to nanoparticles **B**, which do not carry surface reactive functional groups, no monosaccharides were detected, confirming that the sugars were attached to the particles by covalent bonds. TGA showed that negligible amounts of polymeric material had been lost during the chemical modification and purification steps (Figure S16, Supporting Information) indicating that the employed coupling procedures are compatible with the chemical nature of the nanoparticles. Furthermore, the fact that the nucleophilic amine and acylhydrazide moieties of **B** were modified in highly efficient manners supports that these functional groups had remained intact during the preparation of the nanoparticles and had, for example, not reacted with the ester moieties of PCL.

Next, nanoparticles modified by Alexa Fluor 488 were prepared (**D**, Figure 2), containing an additional oligo-arginine peptide (**E**) or a histidine-rich peptide in addition to the latter two probes (**F**). The fluorophore of the particles will make it possible to quantify cellular uptake, the oligo-arginine peptide will facilitate cellular uptake by endocytosis,[19] and the histidine-rich peptide was expected to promote escape of the particles from endosomes and lysosomes.[20] Thus, particles **D**−**F** were expected to differ in cellular uptake and subcellular location. Succinimate ester modified Alexa Fluor probe **14** was selectively linked to the amines of **A** after pretreatment with acetone to block the hydrazines to give **D**. Nanoparticles **D** were the starting material for the preparation of **E** by a Cu(I)-catalyzed reaction of its azides with the oligo-arginine peptide **15** containing an N-terminal alkyne. Nanoparticles **F** were synthesized by first modifying **A** with histidine-rich peptide **13**, which contains an aldehyde function and therefore reacted selectively with the acylhydrazides. Next, the amines of the resulting particles were reacted with **14** under the standard conditions, and finally, the oligo-arginine peptide **15** was installed by Cu(I) catalyzed alkyne−azide cycloaddition to give gold-stabilized and multifunctional particles **F**. Quantitative amino acid analysis and fluorescent intensity measurements showed that the three probes had been incorporated with efficiencies ranging from 55 to 80% (Figure 2b).

Biological Examinations. Having particles **D**−**F** at hand, attention was focused on cellular uptake studies. HeLa cells were exposed to different concentrations of the nanoparticles, and after an incubation time of 5 and 24 h, cell lysates were analyzed for fluorescence intensity. In addition, cells were treated with trypsin[21] prior to hydrolysis and fluorescent measurements to account for the possible presence of cell surface absorbed material. As expected, the presence of the oligo-arginine peptide of nanoparticles **E** and **F** led to a significant increase in cellular uptake compared to the treatment with unmodified particles **A**, and a longer incubation time resulted in increased internalization (Figures 3a and S20, Supporting Information). Furthermore, the treatment with trypsin did not result in a significant reduction in fluorescent intensity indicating that most of the particles had been internalized by the cells. Surprisingly, the presence of the lysosomal escape module of particles **F** (histidine-rich peptide) somewhat lowered the cellular uptake (compared to particles **E** that only contain oligo-arginine moieties). Similar results were obtained when MCF-7 cells were employed.

The intracellular localization of the particles was studied by TEM, which can visualize the gold core of nanoparticles. HeLa cells exposed to unfunctionalized **D** showed only a small number of gold particles (Figure S22, Supporting Information), whereas significant uptake was observed for **E** and **F**, which are modified by a cell permeation peptide (Figures 3b and S23−S25, Supporting Information). As designed, particles **E** and **F** were found in different subcellular locations; **E** was mainly present in vesicular structures, whereas **F** was predominantly found in the cytoplasm and attached to the nuclear membrane. Confocal microscopy also localized **E** in vesicular compartments, whereas **F** was found at the periphery of the nucleus (Figures 3c and S26, Supporting Information), and thus, the TEM and confocal microscopy studies indicate that after an incubation time of 10 h, a significant amount of polymer is still attached to the gold core.

Next, it was examined whether the gold-stabilized nanoparticles can be loaded with a lipophilic drug and whether such a drug

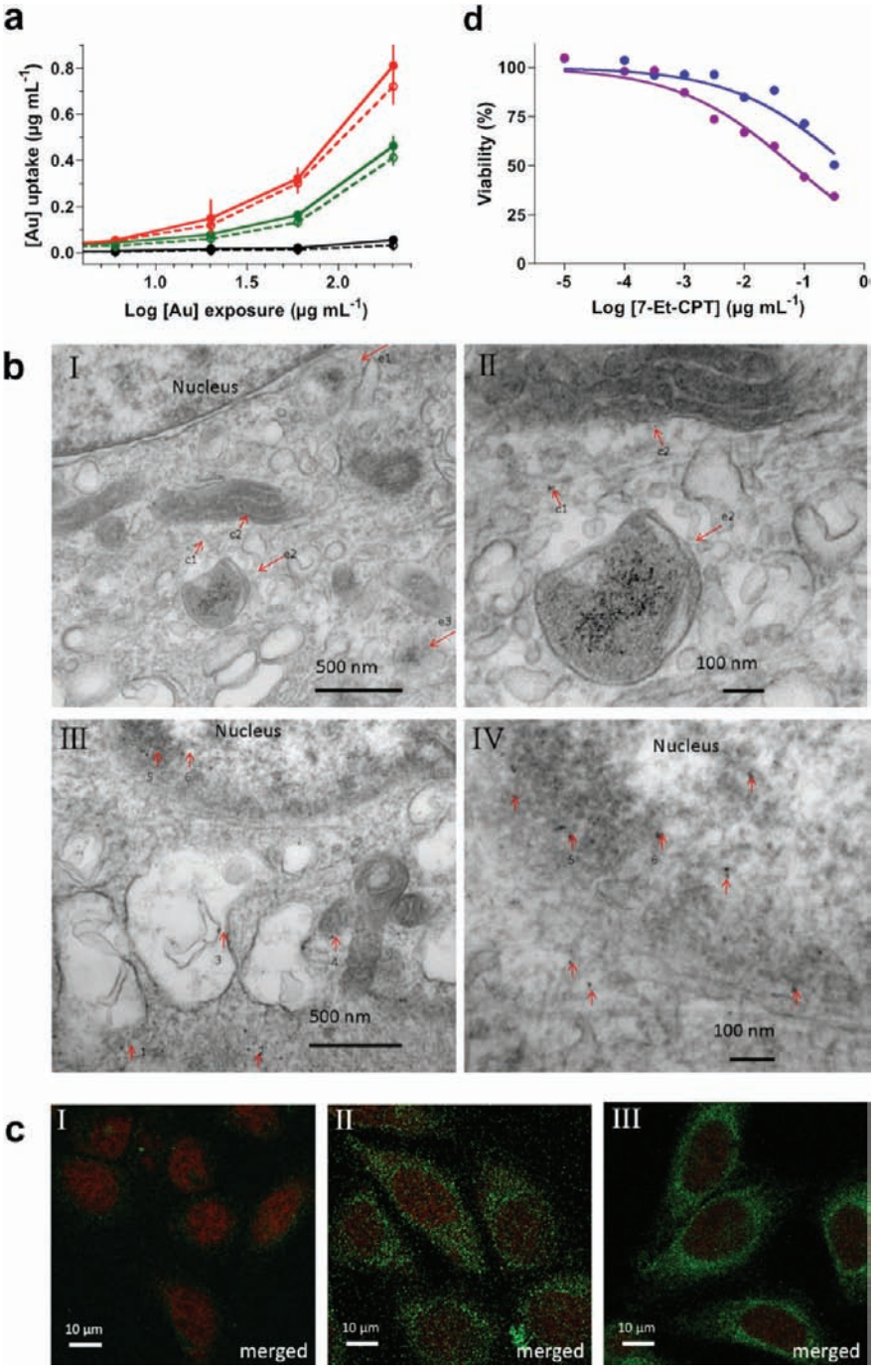

Figure 3. Cellular uptake and cytotoxicity of nanoparticles. HeLa cells were exposed to **D** (black), **E** (red), or **F** (green) at the indicated concentrations of gold for 5 h. After cells were washed and lysed, fluorescence (absorbance 485 nm, emission 520 nm) was measured (solid lines/closed symbols). Samples assessed for internalization were first treated with trypsin before washing and cells lyses (dashed lines/open symbols). Calibration curves of the corresponding Alexa Fluor 488-conjugated gold particles were used to calculate uptake (Figure S19, Supporting Information). Data represent mean values ± SD ($n = 3$) (a). TEM images of representative sections of HeLa cells that were incubated with **E** (I, II) and **F** (III, IV) at 100 μg mL^{-1} gold for 10 h. The endosome is denoted as e and the cytosol as c. Images I and II indicate that nanoparticles **E** are internalized by cells, and the Au NPs were mainly confined in endosomes (arrows e1−3). Only, a very small number of Au NPs were dispersed in the cytosol (arrows c1−3). Images III and IV show that nanoparticles **F** are dispersed in the cytosol (arrow 1), filaments (arrow 2), lysosomes (arrow 3), and mitochondrion (arrow 4), and were especially found around the nuclear membrane (arrow 5) and a few inside the nucleus (arrow 6) (b). Fluorescence images of cells incubated with gold particle preparations **D**−**F**. HeLa cells were exposed to **D** (I), **E** (II), and **F** (III) at 30 μg mL^{-1} gold for 10 h, and after washing, fixing, and staining of the nucleus with the far-red-fluorescent dye TO-PRO-3 iodide, cells were imaged. Merged indicate that the images of cells labeled with Alexa Fluor (488 nm) and TO-PRO iodide (633 nm) are merged and are shown in green and red, respectively (c). Cytotoxicity assessment of 7-Et-CPT-loaded gold nanoparticles **B** and **G**. MCF-7 cells were incubated with 7-Et-CPT-loaded gold nanoparticles **B** (blue) and **G** (purple) at the indicated concentrations of 7-Et-CPT for 8 h. After replacement of the medium, incubation was continued for 3 days. Cell viability values were normalized for untreated control cells (100%). Data represent mean values ± SD ($n = 3$) (d).

dx.doi.org/10.1021/ja2012164 |*J. Am. Chem. Soc.* 2011, 133, 11147–11153

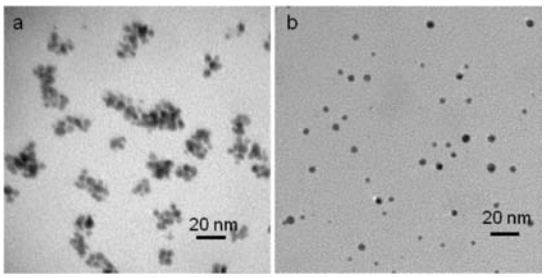

Figure 4. TEM images of gold nanoparticles **B** incubated in the presence (a) or absence (b) of glutathione (10 mM) at 37 °C for 1 week.

can be released after cell entry to exhibit a pharmacological effect. For this purpose, a DMSO solution of 7-ethyl-camptothecin (7-Et-CPT), which is a lipophilic anticancer drug that inhibits topoisomerase I,[22] was added to unmodified (**B**) and particles **G** derivatized with a cell permeation peptide. The resulting preparation was dialyzed, and a loading of approximately 1.5% (w/w of nanoparticles) corresponding to ~70% encapsulation efficiency was determined by fluorescence measurement of a freeze-dried sample redissolved in DMSO. Unloaded particles did not influence cell division of MCF-7 breast cancer cells even at a relatively high concentration of gold (up to 100 μg Au mL^{-1}, Figure S21, Supporting Information), whereas the drug-loaded nanoparticles exhibit dose-dependent cytotoxicity. Furthermore, loaded particles **G** were more potent (IC_{50} = 0.25 μM of 7-Et-CPT) than those of the unmodified and loaded particles **B** (IC_{50} = 1.5 μM). These results indicate that after cell entry, 7-Et-CPT is made available for inhibition. The difference in cytotoxicity of the unmodified and modified particles was not as large as observed for cellular uptake, and this observation is probably due to some leakage of drug from the nanoparticles before cellular uptake. Indeed, it was found that over a period of 24 h, approximately 15% of drug escapes from the particles when dialyzed against water. Many drug delivery systems exhibit such a property and possible remedies include covalent attachment of a drug to the polymers of a nanoparticle preparation.[23] As expected, free 7-Et-CPT (IC_{50} = 0.2 μM, Figure S21, Supporting Information) is slightly more cytotoxic than when loaded in the nanoparticles because it takes a considerable period of time for the drug to escape the particles and be available for inhibiting topoisomerase I. In a clinical setting, slow release may be favorable property, and one of the limitations of cell culture experiments is that it cannot mimic such time frames.

Finally, the influence of glutathione on the polymer layer of the gold nanoparticles was examined. Treatment of nanoparticles **B** in the presence of glutathione (10 mM) at 37 °C for 1 week shifted the surface plasmon peak maximum (λ_{max}) from 526 to 550 nm indicating formation of bulk gold during the agglomeration process. As expected, no change in λ_{max} was observed in the absence of glutathione (Figure S27, Supporting Information). TEM studies also confirmed that glutathione affects nanoparticles **B**, and clusters of Au nanoparticles were formed after 24 h, whereas large aggregates were observed at 72 h (Figures 4 and S28, Supporting Information). Interestingly, these aggregates had a similar morphology as observed for particles internalized by cells. No change in morphology was observed in the absence of glutathione after an incubation time of 3 weeks. The release of 7-Et-CPT in the presence of gluthatione was also examined, however fluorescence quenching of this compound by glutathione, complicated these efforts.

A major objective of nanomedicine is the ability to combine in a controlled manner multiple functions into a single nanoscale entity.[2−8,10] Although previous efforts have resulted in particles with intriguing properties, they were endowed with a limited set of functional properties.[10,24] The gold-stabilized nanoparticles described here have as a unique feature that they can be modified with three different surface modules. Multisurface functionalization will make it possible to target particles with great spatial precision, which is expected to increase the selectivity and potency of therapeutic cargo. For example, one of the modules can target a specific cell type, another one can facilitate cellular uptake, and a third module can direct the particles to a specific subcellular location. As a proof of principle, we have demonstrated that a combined use of a cell permeation and lysosomal escape peptide results in delivery of particles in the cytoplasm. Furthermore, it is to be expected that the specificity of delivery can be enhanced by attachment of several ligands that target a specific cell type. Surface modification post particle synthesis by employing bioorthogonal reactive groups is more attractive than random coupling processes,[25] as it avoids unwanted dispersity. The attraction of the use of a gold core is that it stabilizes the nanoparticles during synthesis so that the various different modules can be attached in a controlled manner without losing the structural integrity of the particles. Furthermore, the gold core ensures controlled degradation after cellular uptake[26] and offers an opportunity for imaging.[27] The apolar polyester layer of the gold-stabilized particle provides a functional loading space for apolar drugs, and PEO corona offers biocompatibility and biological stealthiness.[11] The new synthetic approach makes it also possible to control the surface density of targeting ligand, which in turn is important to achieve optimal selectivity.[13] Finally, the synthetic methodology described here is highly modular, and for the first time, it is possible to prepare from a single platform (e.g., particles **B**), a library of nanoparticles that is modified by different surface entities. It is to be expected that these unique features will make it possible to readily establish optimal configurations of targeted nanoparticle delivery devices.

■ ASSOCIATED CONTENT

Supporting Information. Synthetic procedures and characterization of polymers **1**−**4**; procedures for the preparation of nanoparticles; experimental procedures for nanoparticle characterization including TEM, dynamic light scattering, ζ potential, sugar, amino acid, and biotin quantification; general cell culture protocols; cell-based assays including cellular uptake, TEM imaging of nanoparticle uptake and confocal microscopy; preparation and determination of 7-Et-CPT-loaded nanoparticles; measurement of 7-Et-CPT cytotoxicity; and stability assessment of nanoparticles in the presence of gluthathion. This material is available free of charge via the Internet at http://pubs.acs.org.

■ AUTHOR INFORMATION

Corresponding Author
gjboons@ccrc.uga.edu.

■ ACKNOWLEDGMENT

The authors wish to thank Dr. John Shields (Center for Advanced Ultrastructural Research, University of Georgia) and Mrs. Mary Ard (Electron Microscopy Laboratory, College of

Veterinary Medicine, University of Georgia) for TEM assistance, Prof. Yuesheng Li (Changchun Institute of Applied Chemistry, Chinese Academy of Sciences) for the SEC and TGA measurements, and Dr. Heather Flanagan-Steet for assistance with confocal microscopy studies. This research was supported by the National Cancer Institute of the U.S. National Institutes of Health (grant no. R01 CA88986, G.-J.B.).

REFERENCES

(1) Hawker, C. J.; Wooley, K. L. *Science* **2005**, *309*, 1200–1205.
(2) Peer, D.; Karp, J. M.; Hong, S.; Farokhzad, O. C.; Margalit, R.; Langer, R. *Nat. Nanotechnol.* **2007**, *2*, 751–760. van Dongen, S. F. M.; de Hoog, H. P. M.; Peters, R. J. R. W.; Nallani, M.; Nolte, R. J. M.; van Hest, J. C. M. *Chem. Rev.* **2009**, *109*, 6212–6274. Giljohann, D. A.; Seferos, D. S.; Daniel, W. L.; Massich, M. D.; Patel, P. C.; Mirkin, C. A. *Angew. Chem., Int. Ed.* **2010**, *49*, 3280–3294. Petros, R. A.; DeSimone, J. M. *Nat. Rev. Drug Discovery* **2010**, *9*, 615–627.
(3) Torchilin, V. P. *Pharm. Res.* **2007**, *24*, 1–16.
(4) Boisselier, E.; Astruc, D. *Chem. Soc. Rev.* **2009**, *38*, 1759–1782.
(5) Maeda, H.; Bharate, G. Y.; Daruwalla, J. *Eur. J. Pharm. Biopharm.* **2009**, *71*, 409–419.
(6) Phillips, M. A.; Gran, M. L.; Peppas, N. A. *Nano Today* **2010**, *5*, 143–159.
(7) Torchilin, V. P. *Biopolymers* **2008**, *90*, 604–610.
(8) Rajendran, L.; Knolker, H. J.; Simons, K. *Nat. Rev. Drug Discovery* **2010**, *9*, 29–42.
(9) Jabr-Milane, L.; van Vlerken, L.; Devalapally, H.; Shenoy, D.; Komareddy, S.; Bhavsar, M.; Amiji, M. *J. Controlled Release* **2008**, *130*, 121–128. Torchilin, V. *Eur. J. Pharm. Biopharm.* **2009**, *71*, 431–444.
(10) Sanvicens, N.; Marco, M. P. *Trends Biotechnol.* **2008**, *26*, 425–433.
(11) Owens, D. E.; Peppas, N. A. *Int. J. Pharm.* **2006**, *307*, 93–102.
(12) Sletten, E. M.; Bertozzi, C. R. *Angew. Chem., Int. Ed.* **2009**, *48*, 6974–6998. Kalia, J.; Raines, R. T. *Curr. Org. Chem.* **2010**, *14*, 138–147.
(13) Wang, J.; Tian, S. M.; Petros, R. A.; Napier, M. E.; DeSimone, J. M. *J. Am. Chem. Soc.* **2010**, *132*, 11306–11313.
(14) Brust, M.; Fink, J.; Bethell, D.; Schiffrin, D. J.; Kiely, C. *J. Chem. Soc. Chem. Comm.* **1995**, 1655–1656.
(15) Azzam, T.; Eisenberg, A. *Langmuir* **2007**, *23*, 2126–2132.
(16) Hong, R.; Han, G.; Fernandez, J. M.; Kim, B. J.; Forbes, N. S.; Rotello, V. M. *J. Am. Chem. Soc.* **2006**, *128*, 1078–1079.
(17) Bogdanov, B.; Vidts, A.; van den Bulcke, A.; Verbeeck, R.; Schacht, E. *Polymer* **1998**, *39*, 1631–1636.
(18) Iha, R. K.; Wooley, K. L.; Nystrom, A. M.; Burke, D. J.; Kade, M. J.; Hawker, C. J. *Chem. Rev.* **2009**, *109*, 5620–5686.
(19) Wender, P. A.; Galliher, W. C.; Goun, E. A.; Jones, L. R.; Pillow, T. H. *Adv. Drug Delivery Rev.* **2008**, *60*, 452–472.
(20) Pichon, C.; Goncalves, C.; Midoux, P. *Adv. Drug Delivery Rev.* **2001**, *53*, 75–94.
(21) Richard, J. P.; Melikov, K.; Vives, E.; Ramos, C.; Verbeure, B.; Gait, M. J.; Chernomordik, L. V.; Lebleu, B. *J. Biol. Chem.* **2003**, *278*, 585–590.
(22) Verma, R. P.; Hansch, C. *Chem. Rev.* **2009**, *109*, 213–235.
(23) Sengupta, S.; Eavarone, D.; Capila, I.; Zhao, G.; Watson, N.; Kiziltepe, T.; Sasisekharan, R. *Nature* **2005**, *436*, 568–572. Kolishetti, N.; Dhar, S.; Valencia, P. M.; Lin, L. Q.; Karnik, R.; Lippard, S. J.; Langer, R.; Farokhzad, O. C. *Proc. Natl. Acad. Sci. U.S.A.* **2010**, *107*, 17939–17944.
(24) Pellegrino, T.; Kudera, S.; Liedl, T.; Javier, A. M.; Manna, L.; Parak, W. J. *Small* **2005**, *1*, 48–63. Bertin, P. A.; Gibbs, J. M.; Shen, C. K. F.; Thaxton, C. S.; Russin, W. A.; Mirkin, C. A.; Nguyen, S. T. *J. Am. Chem. Soc.* **2006**, *128*, 4168–4169. Farokhzad, O. C.; Cheng, J. J.; Teply, B. A.; Sherifi, I.; Jon, S.; Kantoff, P. W.; Richie, J. P.; Langer, R. *Proc. Natl. Acad. Sci. U.S.A.* **2006**, *103*, 6315–6320. Nasongkla, N.; Bey, E.; Ren, J. M.; Ai, H.; Khemtong, C.; Guthi, J. S.; Chin, S. F.; Sherry, A. D.; Boothman, D. A.; Gao, J. M. *Nano Lett.* **2006**, *6*, 2427–2430. Medarova, Z.; Pham, W.; Farrar, C.; Petkova, V.; Moore, A. *Nat. Med.* **2007**, *13*, 372–377. Yang, J.; Lee, C. H.; Ko, H. J.; Suh, J. S.; Yoon, H. G.; Lee, K.; Huh, Y. M.; Haam, S. *Angew. Chem., Int. Ed.* **2007**, *46*, 8836–8839. Gao, J. H.; Liang, G. L.; Cheung, J. S.; Pan, Y.; Kuang, Y.; Zhao, F.; Zhang, B.; Zhang, X. X.; Wu, E. X.; Xu, B. *J. Am. Chem. Soc.* **2008**, *130*, 11828–11833. Kim, J.; Kim, H. S.; Lee, N.; Kim, T.; Kim, H.; Yu, T.; Song, I. C.; Moon, W. K.; Hyeon, T. *Angew. Chem., Int. Ed.* **2008**, *47*, 8438–8441. Park, H.; Yang, J.; Seo, S.; Kim, K.; Suh, J.; Kim, D.; Haam, S.; Yoo, K. H. *Small* **2008**, *4*, 192–196.
(25) de la Fuente, J. M.; Barrientos, A. G.; Rojas, T. C.; Rojo, J.; Canada, J.; Fernandez, A.; Penades, S. *Angew. Chem., Int. Ed.* **2001**, *40*, 2258–2261. Garanger, E.; Aikawa, E.; Reynolds, F.; Weissleder, R.; Josephson, L. *Chem. Commun.* **2008**, 4792–4794. Nativo, P.; Prior, I. A.; Brust, M. *ACS Nano* **2008**, *2*, 1639–1644. Zupancich, J. A.; Bates, F. S.; Hillmyer, M. A. *Biomacromolecules* **2009**, *10*, 1554–1563. Kang, B.; Mackey, M. A.; El-Sayed, M. A. *J. Am. Chem. Soc.* **2010**, *132*, 1517–1519.
(26) Kim, C. K.; Ghosh, P.; Pagliuca, C.; Zhu, Z. J.; Menichetti, S.; Rotello, V. M. *J. Am. Chem. Soc.* **2009**, *131*, 1360–1361.
(27) Park, J. H.; von Maltzahn, G.; Ong, L. L.; Centrone, A.; Hatton, T. A.; Ruoslahti, E.; Bhatia, S. N.; Sailor, M. J. *Adv. Mater.* **2010**, *22*, 880–885.